Role of Bloch mode reshaping and disorder correlation length on scattering losses in slow-light photonic crystal waveguides

Nishan Mann,* Mark Patterson, and Stephen Hughes
Department of Physics, Queen's University, Kingston, Ontario, Canada K7L 3N6
(Received 24 October 2014; revised manuscript received 4 May 2015; published 25 June 2015)

Intrinsic disorder in photonic crystal waveguides occurs via rapid fluctuations of the air-dielectric interface and is typically characterized by a quadratic mean surface roughness and a surface correlation length. We theoretically study the impact of correlation length on extrinsic scattering losses and discuss the numerical implementation for several different waveguide designs. The role of correlation length is found to be strongly influenced by the underlying Bloch modes which are dependent on waveguide design and frequency, and can thus be partly controlled via spatial-dispersion engineering. For most frequencies and waveguide designs, we find an asymptotical increase in losses as the correlation length increases; however, we show that for some frequencies and designs, a maximum scattering loss is achieved for a finite correlation length. Our results also demonstrate the importance of choosing an appropriate correlation function for modeling quickly varying disorder.

DOI: 10.1103/PhysRevB.91.245151 PACS number(s): 42.70.Qs, 42.25.Fx, 42.82.Et, 42.81.Dp

I. INTRODUCTION

Photonic crystal waveguides (PCWs) are promising components for integrated optical circuits. Their abilities to guide and slow down light allows for enhanced light-matter interactions [1,2], which have been exploited in various applications such as optical delay lines [3], enhanced nonlinear processes including pulse compression and soliton propagation [4], third-harmonic generation [5], and four-wave mixing [6]. Recently, there has also been considerable work in exploiting PCWs for enabling an on-chip single-photon source [7–10].

The fundamental physics behind photonic crystals (PCs) and photonic band gaps (PBGs) is well understood since the first works by John [11] and Yablonovitch [12], yet there still remains a significant fabrication roadblock to the commercialization of PC devices in integrated optics. In particular, intrinsic disorder introduced at the fabrication stage breaks the periodicity of the PC lattice, which can have a significant impact on the ensuing light-matter interactions and PBG physics. Photonic crystal waveguides are especially sensitive to manufacturing disorder in the slow-light regime, and the detrimental effect on waveguide mode operation is now well known experimentally [13–15] and theoretically [16–20].

In 2005, Hughes *et al.* [16] utilized a photonic Green-function approach to provide an analytical model for understanding the role of disorder-induced scattering losses and subsequently highlighted the detrimental effect for PCWs operating in the slow-light regime. The fabrication disorder was modeled as a quadratic mean surface roughness (rms) appearing on the sidewalls of the etched air holes, and an in-trahole correlation length was included but kept fixed at 40 nm, which is similar to experiments on Si/SiO_2 strip waveguides that show an in-plane correlation length of 50 nm [21]. Related modeling approaches to tackle disorder-induced scattering in PCs were also developed by Johnson *et al.* [18] and Gerace *et al.* [17] around the same time. Gerace *et al.* neglected backscattering losses and computed the radiation losses in PCWs where intrinsic disorder was modeled as a change in the air hole radii. Johnson *et al.* extended the weak-index contrast polarization model used widely in the literature for modeling dielectric perturbations with low-index contrasts (small $\Delta\varepsilon$), to model sidewall/surface roughness in systems such as PCWs where perturbations are rapid and exhibit high-index contrast, which requires a more careful treatment of the surface boundary effects. However, their model can overestimate the scattering losses due to assuming uncorrelated sidewall roughness. For computing losses in finite-length PCWs, the importance of multiple scattering which leads to the formation of disorder-induced localization modes [22] and failure of the Beer-Lambert law was highlighted by Patterson *et al.* [23,24] and also by Mazoyer *et al.* [25].

The effect of scattering losses due to sidewall/surface roughness in the context of single-mode planar optical waveguides was studied decades ago by Marcuse [26], who introduced two statistical parameters to represent the disordered surface: (i) standard deviation of the rapid sidewall roughness (rms roughness) and (ii) correlation length which indicates the length scale over which the sidewall roughness between two points on the sidewall is strongly correlated. Using this surface roughness model, Payne and Lacey [27] studied the impact of these two parameters on extrinsic scattering losses for a simple planar waveguide. Given waveguide parameters and an estimate of the rms roughness, they proved the existence of an upper limit for scattering loss and showed that it occurred for a finite correlation length. Since rms roughness was easier to access experimentally than the correlation length, their formula provided an immediate upper estimate of the expected loss for planar optical waveguides.

Intrinsic fabrication disorder in planar PCWs refers mainly to the deviation of the etched air holes from their ideal cylindrical shape, so the disorder roughness model is significantly more complicated to describe than simple sidewall roughness on a planar waveguide. Given state-of-the-art electron-beam writing and etching techniques, a common approximation for PC slabs with etched holes is to assume the deviated cross section is constant throughout the cylinder's height [16,19], hence one only needs to address in-plane variations. Various other disorder models can be adopted, such as varying only the radius or positions of the holes, though these are less

*nmann@physics.queensu.ca

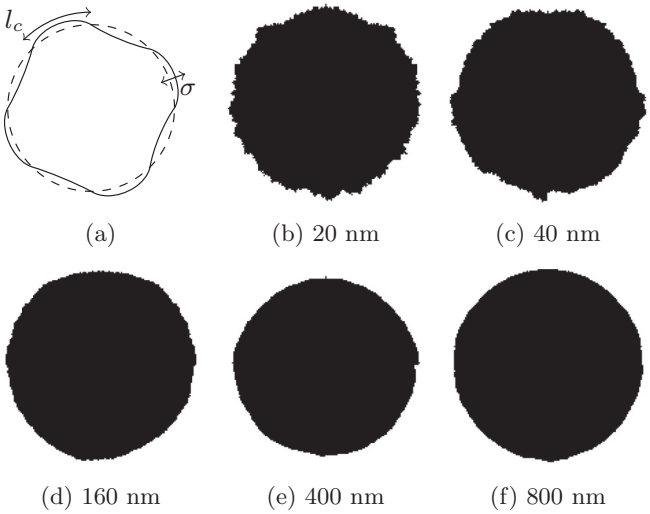

FIG. 1. (a) A schematic showing an ideal cross section of a cylindrical hole (dashed) along with the cross section of a disordered hole (solid). The labels illustrate the statistical parameters used for modeling surface roughness, namely, rms roughness σ and correlation length l_c. (b)–(f) Instances of disordered holes generated using the autocovariance function of Eq. (7). The rms roughness parameter is fixed, $\sigma = 4$ nm, while the correlation length is varied, as shown below in each label. The pitch (hole-to-hole distance along the waveguide) is $a = 420$ nm and the hole has a radius of $0.276a \approx 116$ nm and a circumference of 728 nm.

realistic for modeling intrinsic disorder caused by electron-beam fabrication. One can also introduce deliberate disorder in the design to allow easier access to disorder-induced localization modes [28]. Similar to what is known about standard optical waveguides (e.g., strip and ridge waveguides), we model the surface roughness directly via the standard deviation of the rapid radial fluctuations σ and a correlation length l_c—which in this case is a measure of how strongly two intrahole fluctuations are correlated (disordered holes generated with this model are illustrated in Fig. 1). These two disorder parameters can be estimated from scanning electron microscopy (SEM) images of the PCW samples [29], although an accurate estimate of correlation length is harder to obtain. Often these two parameters can be used as fitting parameters when computing disorder-induced losses in PCWs [16] and comparing to experiment, and good agreement has been found for various PCW material systems and designs [13,23,24,30].

The effect of rms roughness σ on losses is understood as losses increase monotonically as a function of σ [16], i.e., the rougher the hole, the greater the loss (neglecting multiple scattering). However, the effect of correlation length l_c on losses is nontrivial as earlier identified for regular (i.e., non-PC) waveguides by Payne and Lacey [27], and has been partly studied recently for PCWs by O'Faolain *et al.* [31] and Minkov and Savona [32]. Based on a better qualitative explanation for their experimental data, O'Faolain *et al.* proposed that a correlation length of the order of the circumference of the hole (effectively infinity) should perhaps be used for modeling experimental loss characteristics. However, a qualitatively better fit to data does not necessarily justify choosing an unusually large value for the correlation length, since their chosen correlation-length value (∼696 nm) is much larger than typical values (40 to 60 nm) extracted from SEM images of PCWs [29] and used in previous literature reports [16,19]. It is also significantly larger than the correlation lengths for strip waveguides. O'Faolain *et al.* do demonstrate that for the particular reference waveguide that they modeled, a long correlation length can significantly reshape the loss dispersion curve, which is an interesting finding.

Minkov and Savona [32] consider two models for disorder in PCWs. The first model is similar to ours and considers radial fluctuations to be the main source of surface roughness; they find a nontrivial dependence of loss rates on correlation length. The second model considers fluctuations in the hole area, and it was found that varying the correlation length does not have as dramatic an impact on the loss rates as their first model. This latter model for surface roughness was experimentally studied by Le Thomas *et al.* [33] by measuring the correlation between group velocity measurements in disordered PCWs and radial or hole area fluctuations. Operating in the slow-light regime, they found a positive correlation between hole area fluctuations and group velocity, i.e., greater hole area fluctuations lead to a higher group velocity near the cutoff. However, the experimental data was insufficient to determine the correlation between group velocity and radial fluctuations.

Both of these aforementioned papers for modeling the effects of correlation length [31,32] draw their conclusions from a specific PCW design and use only a few values of correlation length. O'Faolain *et al.* [31] studied a modified W1 PCW (a W1 consists of a missing row of holes) and considered only three values for correlation lengths (0, 40, 696 nm); they assumed a step function as the correlation function, though it is not clear how good this approximation is for modeling rapidly varying surface/sidewall roughness. Minkov and Savona used the standard W1 PCW for their calculations and chose only two correlation lengths (5 and 53 nm, assuming a hole radius of 144 nm). They then employed a Gaussian correlation function, which seems like a valid model for describing realistic surface roughness.

In this paper, we adopt the disorder-induced scattering model of Ref. [16], extended to include local-field effects at the interface [18,34] and a changing correlation length. We subsequently carry out a systematic study of the effects of correlation length and explore the impact of PCW design and the underlying Bloch mode on extrinsic scattering losses. We compute the ensemble-averaged backscatter and radiation (out-of-plane) losses, per unit cell, for the PCW, and we discuss the numerical implementation of the model. We do not take into account multiple scattering since the essential features discussed here remain essentially unchanged when one extrapolates losses to a finite-length PCW, and the extension to include multiple scattering is straightforward and documented elsewhere [23]. We study scattering losses as a function of both frequency and correlation length, where the correlation length is varied from a few nm to slightly more than half the circumference of the hole (effectively infinity, see Sec. IV). Importantly, we consider three different PCW designs and find a nontrivial dependence that is sensitive to both frequency and design. In contrast to what was found by O'Faolain *et al.* [31], we find that a longer correlation length does not necessarily yield loss profiles with significantly

different features. Moreover, unlike Minkov and Savona's work [32] on a specific W1 PCW, where increasing correlation length leads to an increase in loss rates, we observe that for some frequencies and designs, there exists a maximum loss that is reached for a finite correlation length (∼100 nm), in line with Payne and Lacey's finding for regular ridge waveguides [27]. For other frequencies and designs, we observe an asymptotical increase in loss as the correlation length increases. These trends are caused by the quickly varying amplitude and phase of the Bloch mode field around the hole circumference. The Bloch modes are highly design and frequency dependent, which we refer to as *Bloch mode reshaping*. Our findings demonstrate the important role of the Bloch modes in determining the loss behavior, and lead to an increased understanding of the role of correlation-length disorder in these systems.

The layout of the remainder of our paper is as follows: in Sec. II, we review our modeling approach for computing the disorder-induced backscatter and radiation losses, and include a discussion of the disorder polarization model employed. In Sec. III, we present our results showing the impact of correlation length on losses for three different PCW designs and for various correlation lengths. Section IV examines the dependence of our results on Bloch mode reshaping, and in Sec. V we discuss our findings in the context of the previous literature. Finally, we give our conclusions in Sec. VI.

II. THEORY OF DISORDER-INDUCED SCATTERING LOSSES

Disorder-induced losses in PCWs can be divided into two main loss channels, backscattering loss and radiation loss, with backscattering being the dominant loss mechanism for slow-light waveguides (as also shown in Fig. 4). Backscattering losses occur due to coupling between the forward- and backward-propagating Bloch modes, while radiation losses are due to coupling between the propagating Bloch mode and radiation modes above the light line. Treating structural disorder as a perturbation which gives rise to macroscopic polarization density function $\mathbf{P}(\mathbf{r},\omega)$, we start with the Dyson equation which is a self-consistent, nonperturbative solution for the electric field $\mathbf{E}(\mathbf{r},\omega)$ in the disordered system,

$$\mathbf{E}(\mathbf{r},\omega) = \mathbf{E}_0(\mathbf{r},\omega) + \int \overleftrightarrow{\mathbf{G}}(\mathbf{r},\mathbf{r}',\omega)\cdot\mathbf{P}(\mathbf{r}',\omega)d\mathbf{r}', \qquad (1)$$

where $\mathbf{E}_0(\mathbf{r},\omega)$ is the unperturbed electric field and $\overleftrightarrow{\mathbf{G}}(\mathbf{r},\mathbf{r}',\omega)$ denotes the Green function or tensor satisfying the following wave equation,

$$\nabla\times\nabla\times\overleftrightarrow{\mathbf{G}}(\mathbf{r},\mathbf{r}',\omega) - \frac{\omega^2}{c^2}\varepsilon(\mathbf{r})\overleftrightarrow{\mathbf{G}}(\mathbf{r},\mathbf{r}',\omega) = \frac{\omega^2}{c^2}\delta(\mathbf{r}-\mathbf{r}')\overleftrightarrow{\mathbf{I}}, \qquad (2)$$

where $\overleftrightarrow{\mathbf{I}}$ is the unit dyadic, $\varepsilon(\mathbf{r})$ is the ideal dielectric constant profile of the PCW, and $G_{ij}(\mathbf{r},\mathbf{r}',\omega)$ is the ith component of the electric field at $\mathbf{r}$ that arises in response to a j polarized point dipole at $\mathbf{r}'$ with angular frequency ω. Since $\mathbf{P}\propto\mathbf{E}$, we iterate the solution to second order (perturbative Born approximation) to derive the ensemble-averaged backscattering power loss, per unit cell, which is given by (the ω dependence is implicit) [16]

$$\langle\alpha_{\text{back}}\rangle = \left(\frac{a\omega}{2v_g}\right)^2 \iint_{\text{cell}} d\mathbf{r}d\mathbf{r}'\,\langle[\mathbf{E}(\mathbf{r})\cdot\mathbf{P}(\mathbf{r})][\mathbf{E}^*(\mathbf{r}')\cdot\mathbf{P}^*(\mathbf{r}')]\rangle\,, \qquad (3)$$

where $\mathbf{E}(\mathbf{r}) = \mathbf{e}_k(\mathbf{r})e^{ikx}$, $\mathbf{e}_k(\mathbf{r})$ is the Bloch mode, x denotes the direction of the waveguide, a is the pitch, v_g is the group velocity, and $\mathbf{P}(\mathbf{r})$ represents the structural disorder (i.e., this is zero for a perfect PC lattice). The Bloch modes are normalized through $\iint_{\text{cell}}\varepsilon(\mathbf{r})|\mathbf{e}_k(\mathbf{r})|^2 = 1$ and the bracket term $\langle\cdots\rangle$ refers to the expectation or an ensemble average over nominally identical disordered waveguides. The polarization term representing structural disorder accounts for a quickly varying dielectric perturbation around the hole surfaces, as shown in Fig. 1. Lastly, the ensemble-averaged radiation loss per unit cell, $\langle\alpha_{\text{rad}}\rangle$, is derived similarly [23] and is given by

$$\langle\alpha_{\text{rad}}\rangle = \frac{a\omega}{v_g}\iint_{\text{cell}} d\mathbf{r}d\mathbf{r}'\,\langle\mathbf{P}^*(\mathbf{r}')\cdot\text{Im}[\overleftrightarrow{\mathbf{G}}_{\text{rad}}(\mathbf{r},\mathbf{r}';\omega)]\cdot\mathbf{P}(\mathbf{r})\rangle\,, \qquad (4)$$

where Im[$\cdots$] denotes the imaginary part, and $\overleftrightarrow{\mathbf{G}}_{\text{rad}}$ denotes the radiation contribution to the total Green function of the PCW. The details for approximating $\overleftrightarrow{\mathbf{G}}_{\text{rad}}$ for a PCW are discussed in Ref. [35], and it essentially accounts for scattering out of the PCW via the continuum of radiation modes above the light line. A particularly attractive feature of

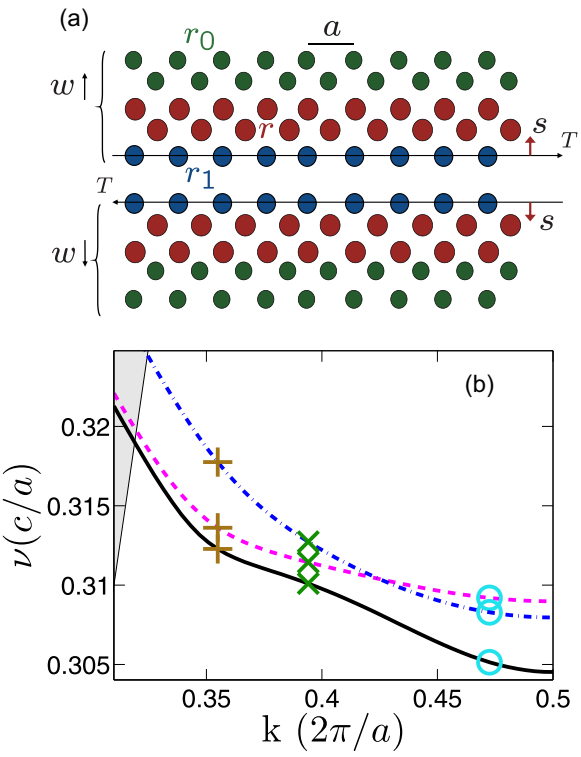

FIG. 2. (Color online) (a) Schematic of the PCW designs, with the parameters given in Table I. (b) Band structure for the fundamental TE-like guided mode for all three designs: W1 (blue dot-dashed line), WG2 (thick black solid line), WG3 (magenta dashed line). The light line is marked by the thin black solid line and the markers correspond to the frequencies for which Bloch modes are shown in Fig. 3.

TABLE I. Parameters illustrated in Fig. 2(a) for the three different waveguides considered in this work.

	a (nm)	$r_0\,(a)$	$r_1\,(a)$	$r\,(a)$	$w\left(\frac{\sqrt{3}}{2}a\right)$	$s\left(\frac{\sqrt{3}}{2}a\right)$	$T(a)$	$h(a)$
W1	480	0.2	0.2	0.2	0.0	0.0	0.0	0.333
WG2	482	0.23	0.25	0.26	−0.1	0.16	0.15	0.367
WG3	477	0.23	0.25	0.26	−0.1	0.18	0.0	0.367

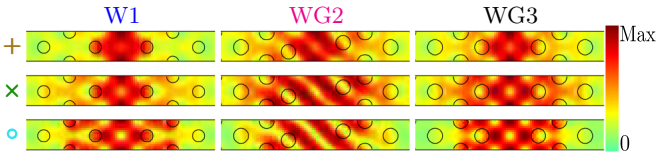

FIG. 3. (Color online) The Bloch mode intensity $|\mathbf{e}_k|^2$ in a horizontal slice in the center of the slab for the three frequencies and PCW designs marked in Fig. 2(b). As indicated by the markers (+, ×, ∘), the wave vector k is kept fixed in each horizontal panel as it approaches the mode edge from top to bottom in each vertical panel.

our model is that it uses the unperturbed Bloch modes and band structure of the PCW as input, and these are straightforward to calculate since various efficient numerical algorithms for solving Maxwell equations in periodic media already exist in the literature [36]. Such an approach not only helps to identify the underlying physics of disorder-induced scattering, but has been successfully used to model a variety of related experiments [13,23,24,30,31].

The disorder polarization term $\mathbf{P}(\mathbf{r})$ arising from a disordered element at $\mathbf{r}'$ is given by [18,34]

$$\mathbf{P}(\mathbf{r}) = \left[\left(\frac{\varepsilon_1+\varepsilon_2}{2}\right)\alpha_\parallel \mathbf{E}_\parallel(\mathbf{r}) + \varepsilon(\mathbf{r})\gamma_\perp \mathbf{D}_\perp(\mathbf{r})\right]\Delta V\delta(\mathbf{r}-\mathbf{r}'), \tag{5}$$

where $\varepsilon_{1,2}$ are the dielectric constants for air and the underlying slab, respectively, $\alpha_\parallel, \gamma_\perp$ are the polarizability tensors representing the disordered element and $\mathbf{E}_\parallel$, $\mathbf{D}_\perp = \varepsilon(\mathbf{r})\mathbf{E}_\perp$ are the parallel and perpendicular components, respectively, of the ideal electric/displacement fields at the air-slab dielectric interface, and ΔV is the volume of the disorder element. Unlike the weak-index contrast model $\mathbf{P} = \Delta\varepsilon\mathbf{E}$, which is known to be ill defined in high-index contrast structures such as PCWs [18,37], the local fields in this model are well defined at dielectric interfaces with high-index contrast. While the more traditional slowly varying surface model introduced earlier by Johnson *et al.* [37], and employed in Ref. [19], is also well defined at dielectric interfaces, our model is more suited to intrinsic PCW disorder as it models the quickly varying surface of the disordered hole through its asymmetric numerical polarizability tensors. Apart from computing experimentally relevant losses without problematic polarization components at the interface, this model also predicts a nonzero first-order resonance frequency shift [34], in good agreement with recent experiments [38,39].

Since we assume a constant cross section for the disorder element, ΔV is replaced by the cross-sectional area ΔA of the disordered element [18] in Eq. (5). Since $\Delta A \ll A$, it is sufficient to consider only the lowest-order term in the expression of ΔA which is proportional to $|\Delta r|$, the magnitude of the rapid intrahole radial fluctuations. Under these assumptions, Eq. (5) is slightly modified [18] and, by inserting this into Eq. (3), one can show that Eq. (3) is reduced to a line integral around the cylindrical circumference of each hole in the unit cell. To abbreviate notation, we denote $f(\mathbf{r}) \equiv f$, $f(\mathbf{r}') \equiv f'$, $e_\parallel^2 \equiv \mathbf{e}_{k\parallel}\cdot\mathbf{e}_{k\parallel}$, $d_\perp^2 \equiv \mathbf{d}_{k\perp}\cdot\mathbf{d}_{k\perp}$, where the dot product is defined in Ref. [40]. Thus the backscatter loss expression is given by

$$\langle\alpha_{\text{back}}\rangle = \left(\frac{a\omega}{2v_g}\right)^2 \sum_m \int_{\Omega_m}\int_{\Omega_m} d\mathbf{r}d\mathbf{r}' e^{i2k(x-x')}\big[\varepsilon_{\text{av}}^2\,\langle\alpha_\parallel|\Delta r|\alpha_\parallel'|\Delta r'|\rangle\, e_\parallel^2 e_\parallel^{'*2} + \langle\gamma_\perp|\Delta r|\gamma_\perp'|\Delta r'|\rangle\, d_\perp^2 d_\perp^{'*2}$$
$$+ \varepsilon_{\text{av}}(\langle\alpha_\parallel|\Delta r|\gamma_\perp'|\Delta r'|\rangle\, e_\parallel^2 d_\perp^{'*2} + \langle\gamma_\perp|\Delta r|\alpha_\parallel'|\Delta r'|\rangle\, d_\perp^2 e_\parallel^{'*2})\big], \tag{6}$$

where Ω_m denotes the cylindrical boundary of the mth hole in the ideal PCW and $\varepsilon_{\text{av}} = (\frac{\varepsilon_1+\varepsilon_2}{2})$. The numerical polarizability tensors depend on the sign of the radial fluctuation, where $\Delta r > 0$ denotes a bump into the slab and vice versa, and $\alpha_\parallel[\text{sgn}(\Delta r)], \gamma_\perp[\text{sgn}(\Delta r)]$ where $\text{sgn}(x)$ is the standard sign function; the polarizability tensors are computed using the formulas given in Johnson *et al.* [18]. In cylindrical coordinates, where θ denotes the polar angle and z denotes the height, the random radial fluctuations are assumed to vary as a function of polar angle only, $\Delta r(\theta)$. The radial fluctuations are modeled as a Gaussian stochastic process which is determined by its first-order (mean) and second-order (standard deviation σ) moments. Also consistent with experimental data, intrahole fluctuations are assumed to be correlated; so we introduce the correlation length l_c, as a measure of the arc length over which two points on the hole surface are strongly correlated to each other. The mean of the fluctuations is assumed to be zero and the correlation length can be estimated from SEM images [29]. The autocovariance function given below, between any two points on a hole of radius r_m, is adapted from the works of Marcuse [26] and Payne and Lacey [27] in the field of optical waveguides, and is given by

$$\langle\Delta r(\theta)\Delta r(\theta')\rangle = \sigma^2 e^{-r_m|\theta-\theta'|/l_c}. \tag{7}$$

This allows one to generate various instances of disordered holes, as shown in Figs. 1(b)–1(f). A valid autocovariance function regardless of the functional form must have two features in common [26], for $|\theta-\theta'| \to 0$, it must reach its maximum and vanish as $|\theta-\theta'| \to \infty$. While rms roughness σ controls the magnitude of the roughness, the role of correlation length is more subtle. For a fixed σ, as $l_c \to 0$, the hole gets rougher to the point where no two points are

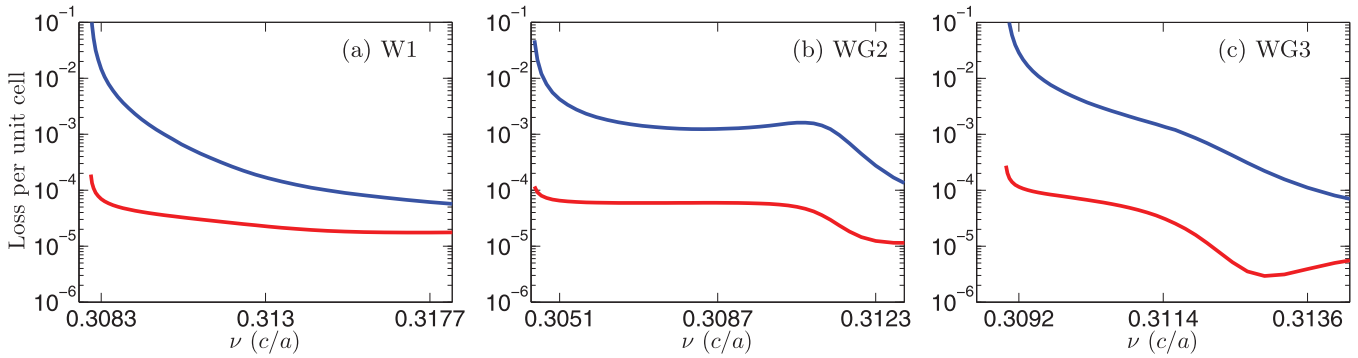

FIG. 4. (Color online) (a)–(c) Backscatter (upper blue solid line) and radiation losses (lower red solid line) per unit cell on a semi-logarithmic scale for all three designs with a fixed correlation length of 40 nm.

correlated, as shown approximately in Fig. 1(b), and as $l_c \rightarrow \infty$, all points on the hole become perfectly correlated so only the radius of the hole changes, as shown in Fig. 1(f). Lastly, the correlation function is contained within the expression of Eq. (7) and in this case is given by $e^{-r_m|\theta-\theta'|/l_c}$.

III. RESULTS FOR DISORDER-INDUCED LOSSES AND HOW THEY DEPEND ON CORRELATION LENGTH AND DESIGN

Loss characteristics for three different PCW designs are studied as a function of correlation length and frequency. Two of the designs are so-called dispersion engineered (DE) by manipulating some of the hole positions in the periodic lattice, and the third design is the standard reference. The two other PCWs are referred to here as WG2 and WG3, respectively. Dispersion engineering is achieved by tailoring the dispersion via geometrical modifications of the underlying periodical dielectric structure with the intent of better designing the slow-light nature of the PCW. This is mainly accomplished through two intertwined features: minimizing group velocity dispersion (GVD) over a finite range of frequencies [41], giving one a better delay bandwidth product, and designing slow-light regions away from the mode edge [42]. The two chosen DE designs (WG2 and WG3) were experimentally demonstrated by Sancho *et al.* [3] to have an improved delay bandwidth product and lower power losses than the reference W1 design. The reduction in loss was found to be due to Bloch mode spatial reshaping, which lowered the field amplitude around the hole circumference, and hence minimizes the loss integral term in Eq. (3) [30]. A schematic illustrating the geometrical modifications, tailored band structures, and modes for all waveguides is shown in Figs. 2 and 3.

The structural parameters for the three waveguides are given in Table I, where h denotes the thickness of the PC slab. Given an average pitch (a) of 480 nm, the typical circumference of a hole in our designs is approximately 663 nm. We use a rms roughness value of $\sigma = 4$ nm and vary the correlation length from 40 to 400 nm ($\sim 0.08a$–$0.83a$). We employ the polarization model introduced in Sec. II to compute the ensemble-averaged backscatter and radiation losses per unit cell for all three designs. For numerical calculations, the band structure and eigenmodes of Maxwell's equations for the fundamental unit cell of an ideal PCW were computed by the MIT PHOTONIC-BANDS (MPB) [36] package, and the integration in Eqs. (3) and (4) is carried out numerically using a double Riemann sum with step sizes of 5 and 28 nm in the azimuthal and vertical directions, respectively. These spatial step sizes were checked to be sufficiently small to ensure numerical convergence for the spatial integrals. For all three designs, we compare the backscatter and radiation losses using a semi-logarithmic scale in Fig. 4 given a correlation length of 40 nm, a typical value used in our previous works [16,23,30]. We see that for all chosen frequencies and PCW designs, radiation losses are at least an order of magnitude lower than backscattering losses, so their precise behavior as a function of correlation length is less important. Therefore, we will focus on backscattering losses for the rest of the paper.

Figure 5 plots the backscatter losses per unit cell, respectively, for two different correlation lengths, 100 and 400 nm. As shown in Figs. 6(a)–6(c), for each waveguide we pick three frequencies of interest: one near the mode edge ($k \approx 0.5$), one near the light line ($k \approx 0.3$), and one lying approximately in the middle of these two extremes. Figures 6(d)–6(f) plot the backscatter loss normalized by n_g^2 (n_g denotes the group index) as a function of correlation length for these frequencies. By removing the group index scaling, we are focusing on the contribution of the integral term of Eq. (3) which highlights the interplay between the normalized Bloch modes and the correlation function. As shown in Figs. 5 and 6, independent of waveguide design, for frequencies lying close to the mode edge, backscatter loss increases asymptotically as the correlation length increases and similarly for frequencies far away from the mode edge lying near the light line. For W1 and WG3 designs, for $\nu(c/a) \approx 0.3127$, 0.3114, respectively, in Figs. 5(d) and 5(f), we observe a deviation in this behavior, shown more clearly in Figs. 6(d) and 6(f) as the backscatter loss reaches a maximum for $l_c \approx 100$ nm and then decreases towards an asymptotic value as the correlation length increases. This is in line with the previous work of Payne and Lacey [27], who also observed a peak in radiation losses as a function of correlation length in regular optical waveguides. In stark contrast, the WG2 design exhibits no such maximum as the behavior is similar to the other two frequencies. A peak in the backscatter loss is caused by the interplay between the correlation function and the field terms $e_\parallel^2 e_\parallel^{'*2}$, $d_\perp^2 d_\perp^{'*2}$, $e_\parallel^2 d_\perp^{'*2}$, $d_\perp^2 e_\parallel^{'*2}$. of Eq. (6), which are implicitly dependent on the amplitude and phase of the Bloch mode around the holes.

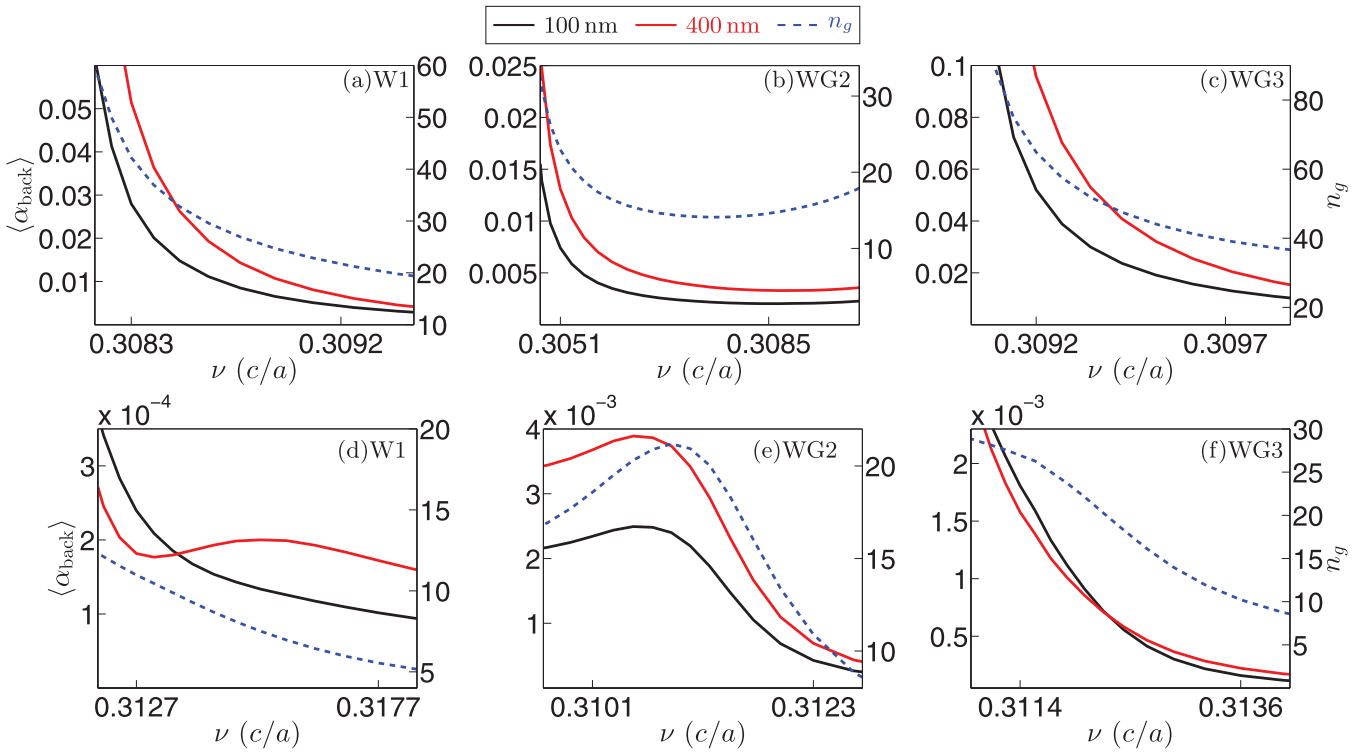

FIG. 5. (Color online) Backscatter losses per unit cell vs frequency for two correlation lengths, 100 and 400 nm, and three different PCW designs where the hole circumferences range from around 600 to 700 nm. For each design, (a)–(c) show frequencies near the mode edge, while frequencies near the light line and in between the light line and mode edge are shown in (d)–(f). The group index vs frequency is shown by the blue dashed curve.

The behavior of backscatter loss for a correlation length of 400 nm resembles $l_c \to \infty$ since the correlation length is greater than half the circumference of the hole (see Sec. IV) and we see from Figs. 6(d)–6(f) that independent of the frequency or design, the losses approach a finite limit. On the other hand, as $l_c \to 0$, backscatter loss depends on the polarization model employed. To examine this limit numerically, we employ a Riemann sum which is a first-order approximation where the numerical error Δ is of the order of the spatial step size $\Delta \sim O(\delta r)$. If the target numerical error is less than the correlation length $\Delta < O(l_c)$, then one can show that the step size must be less than the correlation length $\delta r < O(l_c)$. Therefore, given a step size δr, the lowest correlation length one can study numerically is the order of the step size. Our numerical step size in the azimuthal direction is approximately 5 nm. For the polarization model employed here, the backscatter loss decreases to a positive definite value theoretically as $l_c \to 0$, as one can see if one extrapolate the curves in Figs. 6(d)–6(f). For weak-index and smooth surface polarization models employed previously [16,19], the backscatter loss vanishes, as $l_c \to 0$ theoretically but numerically is limited by a finite grid size, as shown in Fig. 7.

To summarize, the backscatter loss dependence on correlation length is nontrivial and highly dependent on the underlying Bloch mode spatial profiles. In addition, we do not find that a longer correlation length necessarily yields a significantly different loss profile as reported in Ref. [31] for a specific design. While there are subtle differences as the correlation length varies, we find that the essential features of the loss profile remain largely unchanged (e.g., the loss increases dramatically as one approaches the mode edge for all correlation lengths). Since the choice of correlation length should be guided by SEM images of real samples and similar correlation lengths have been reported for silicon ridge waveguides [21], it seems not too surprising that a value of 40 nm has been a good estimate to use in a model for computing experimentally relevant loss values for PC waveguides having a pitch of around 480 nm.

IV. INTERPLAY BETWEEN THE CORRELATION FUNCTION AND BLOCH MODES

We have studied and shown a nontrivial dependence of losses on correlation length for three different PCW designs and frequencies. The qualitatively different behaviors are caused by strong Bloch mode reshaping occurring in DE PCWs, which we will study in more detail in this section. We have varied the correlation length systematically (effectively from near zero to infinity) and found that for some designs and frequencies, such as the reference W1 and WG3, there exists a maximum loss which is reached for a finite correlation length ($\approx$100 nm), while for the WG2 design, the losses increase asymptotically as the correlation length increases. As remarked above, similar behavior was also observed in regular dielectric waveguides by Payne and Lacey [27], but in their case the upper limit for loss was shown to be dependent on the Fourier transform of the correlation function and completely independent of the waveguide mode since it is constant on the

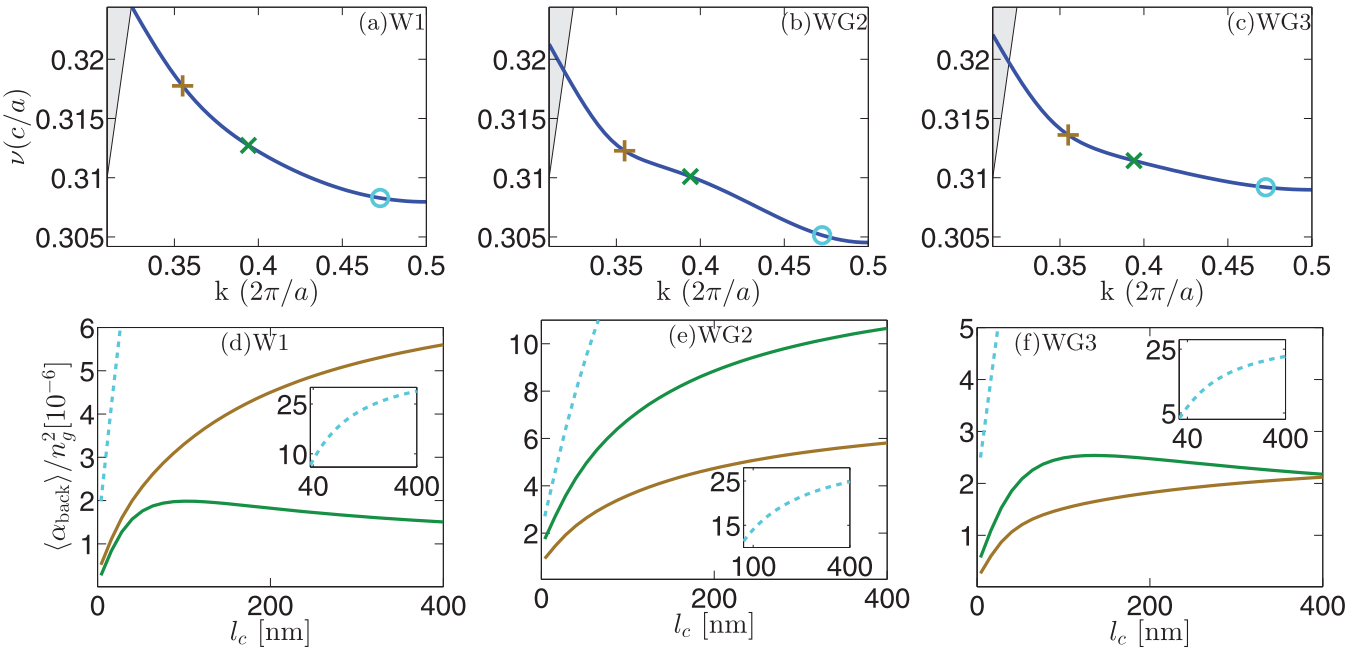

FIG. 6. (Color online) (a)–(c) For reference, here we show the band structure of the fundamental TE-like waveguide mode for all three designs marking the different frequency points: near light line (+), between light line and mode edge (×), and near mode edge (○). (d)–(f) Highlighting the effect of the integral term in Eq. (3), the backscatter loss normalized by n_g^2 is plotted as a function of correlation length for frequencies marked in (a)–(c). Insets: continuation of the cyan dashed curve.

sidewalls of a planar waveguide. Unlike dielectric waveguides, backscatter loss in PCWs is highly dependent on the quickly varying Bloch modes on the hole boundary, as shown in Eq. (6) and Fig. 3. To help understand this hypothesis, we now study the contribution of both the phase and amplitude of the Bloch modes on backscatter loss in PCWs.

For simplicity, we use the weak-index contrast polarization model for disorder (i.e., $\mathbf{P} = \Delta\varepsilon\mathbf{E}$) [16] to examine the effect of the integral term in Eq. (3) since the integral takes a much simpler form compared to Eq. (6) and the trends observed in the previous section remain unchanged. Approximating further, we consider only the two holes closest to the line defect since most of the Bloch mode intensity is concentrated there (see Fig. 3). Under these assumptions, denoting I_0 as the integral contribution to the backscatter loss, the basic loss characteristics of Eq. (3) can be written as

$$I_0 = \int_{\Omega_0}\int_{\Omega_0} d\mathbf{r}d\mathbf{r}' e^{-r_0|\theta-\theta'|/l_c} e^{i2k(x-x')} e_k^2 e_k'^{*2}, \qquad (8)$$

where r_0 is the radius of the nearest hole. We note that e_k^2 is an implicit function of the Bloch mode phase and amplitude and, using the triangle inequality, one can show that $|e_k^2| \leqslant |\mathbf{e}_k|^2$. Figures 7(a)–7(c) plot $I_0(l_c,\nu)/\max(I_0)$ for the three frequencies considered in Fig. 6. Normalizing the integral to unity allows one to identify the trends for comparison with the results of the previous section. Since Figs. 7(a)–7(c) and Figs. 6(d)–6(f) are qualitatively similar, it is thus sufficient to consider the Bloch mode profiles around the two nearest holes (to the line defect).

We now examine the effect of the amplitude ($|e_k^2|$) and phase (ϕ) on backscatter loss by writing e_k^2 in polar form as $e_k^2 = |e_k^2|e^{i\phi}$. By neglecting the phase, Eq. (8) becomes

$$I_a = \int_{\Omega_0}\int_{\Omega_0} d\mathbf{r}d\mathbf{r}' e^{-r_0|\theta-\theta'|/l_c} e^{i2k(x-x')} \left|e_k^2\right|\left|e_k'^2\right|. \qquad (9)$$

Figures 7(d)–7(f) plot $I_a(l_c,\nu)/\max(I_a)$ for the selected three frequencies and designs. Since the amplitude is a positive definite quantity, we observe a monotonic increase as the correlation length increases. Hence the Bloch mode amplitudes are not enough to explain the trends observed in the previous section. If we now neglect the amplitude (i.e., consider only the phase), the integral from Eq. (8) becomes

$$I_p = \int_{\Omega_0}\int_{\Omega_0} d\mathbf{r}d\mathbf{r}' e^{-r_0|\theta-\theta'|/l_c} e^{i2k(x-x')} e^{i(\phi-\phi')}, \qquad (10)$$

and we plot $I_p(l_c,\nu)/\max(I_p)$ in Figs. 7(g)–7(i). In comparison with Fig. 6, the trends for all frequencies agree well for the W1 and WG2 designs, but for the WG3 design, where the existence of a maximum is not observed. This leads us to conclude that, in general, both the phase and amplitude of the Bloch modes around the holes (implicit in the term e_k^2) are needed to explain our findings.

The correlation function is responsible for defining an approximate domain of integration. Since the fields are relatively constant in the vertical direction, we only consider in-plane integration for the current discussion. The domain (θ,θ') satisfying $e^{-r_0|\theta-\theta'|/l_c} \in [1,\frac{1}{e}]$ is important because the integral of Eq. (8) approximately vanishes outside this domain. We note that for $l_c \geqslant C/2$, where C denotes the circumference of the hole, the domain encompasses the complete hole, i.e., $\theta,\theta' \in [-\pi,\pi]$. Hence, given a correlation length, the correlation function defines a domain of integration where

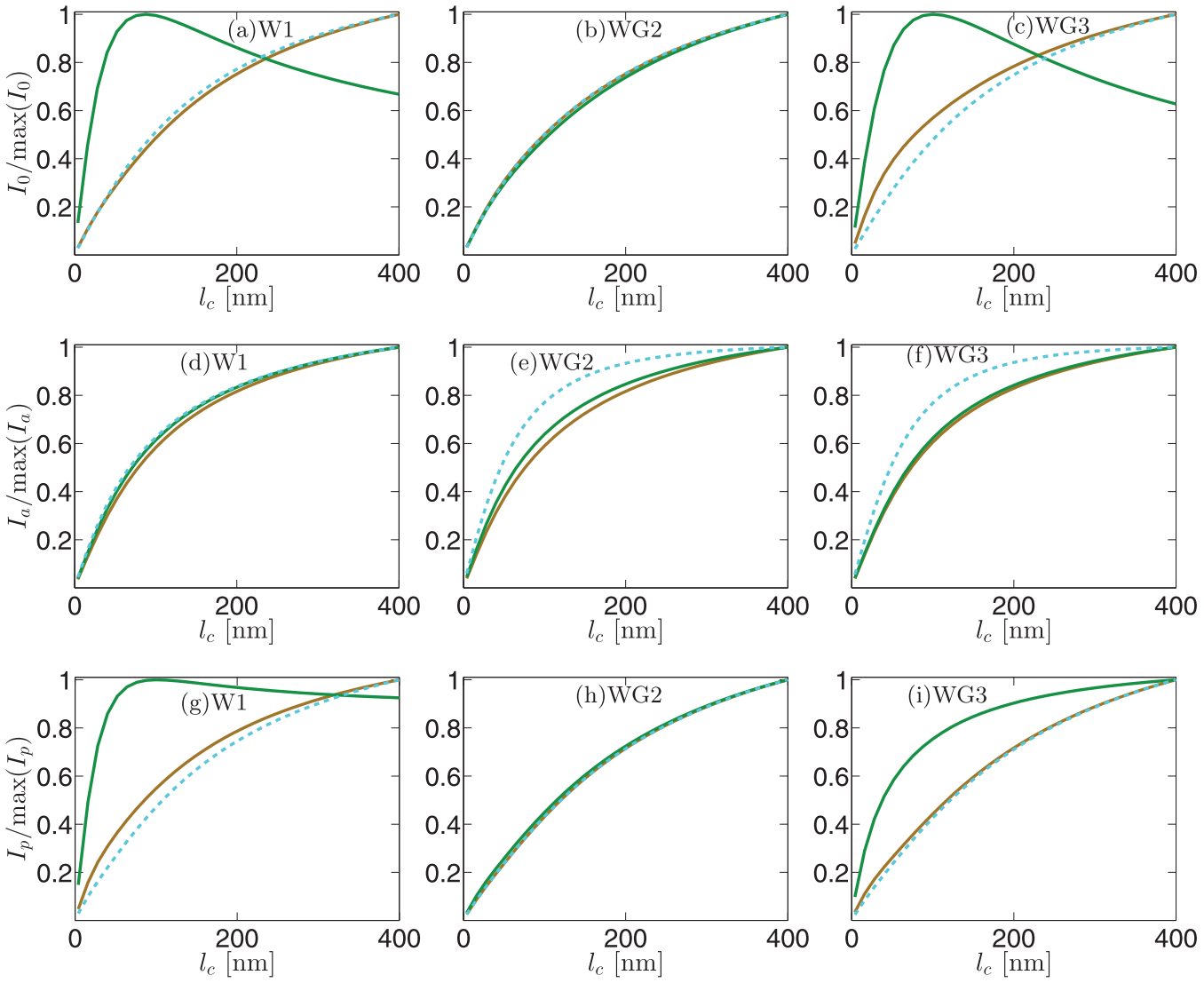

FIG. 7. (Color online) The integral term [Eq. (8)] in the backscatter loss expression [Eq. (3)] as a function of correlation length is studied under various approximations as discussed in Sec. IV, for the same frequencies marked in Figs. 6(a)–6(c). (a)–(c) Contribution of the two nearest holes (to the line defect) including the full Bloch modes. (d)–(f) Here we neglect the phase and consider only the amplitude of e_k^2 around the two nearest holes, through Eq. (9). (g)–(i) Next, we neglect the amplitude and consider only the phase of e_k^2 around the two nearest holes, through Eq. (10).

intrahole interference $e_k^2 e_k^{\prime *2}$ plays an important role. For a finite correlation length and for certain frequencies and PCW designs, the intrahole interference is constructive and maximal over the domain of integration, leading to a maximum in backscatter loss. Physically this is similar to the transmission maximum of an antireflection coating caused by varying the thickness of the thin film, though clearly complicated by the field profiles and the hole structure of our PCWs.

V. DISCUSSION

It is useful to compare our results to previous works in the literature. In Ref. [31], it was suggested that correlation length of the order of the circumference of the hole (effectively infinity) should be used to compute a loss profile that accurately captures the essential features observed in experiments. Their model is derived from the work of Wang *et al.* [19] with similar prefactors as in Eq. (3); the integral term in their backscatter loss expression is given by $\sum_n |\int_{l_c} \alpha(\mathbf{r}) d\mathbf{r}|^2$, where $\alpha(\mathbf{r}) = \mathbf{E}_\parallel \cdot \mathbf{E}_\parallel + \frac{1}{\varepsilon_1 \varepsilon_2} \mathbf{D}_\perp \cdot \mathbf{D}_\perp$, and the hole is divided into n parts of length l_c and the fields are integrated over these line segments. This approach is clearly not the same as our nonseparable double spatial integration, as is shown in Eq. (6). To the best of our understanding, the expression above is derived assuming the correlation function is a step function, where l_c denotes the correlation length over which radial fluctuations are perfectly correlated (unity) and uncorrelated everywhere else (zero) outside of the segment. It is not clear why points within these segments will not be correlated with neighboring segments, and such a model cannot be derived from the typical Gaussian or exponential functions for the intrahole correlation. This may explain why O'Faolain *et al.* [31] notice such an

unusually strong dependence in their loss behavior when the correlation length is changed from 40 nm to effectively infinity.

However, as mentioned in Sec. II, all correlation functions approach unity as the correlation length approaches infinity and the coupled double integral in Eq. (3) is then separable and the field is integrated coherently around the entire hole circumference. The disorder model then becomes equivalent to the size disorder model, which only models changes in the hole radii. As stated in Ref. [19], this simplified model captures the qualitative loss behavior and O'Faolain *et al.* [31] findings demonstrate this for their DE PCW designs.

The other recent work on the role of correlation length is by Minkov and Savona [32], who study the effect of correlation length on loss rates that include both backscatter and out-of-plane losses. They consider two different disorder models for modeling a quickly varying hole surface, namely, the standard rapid radial fluctuations which we employ in this work and rapid fluctuations of the hole area. For the first model, they find that losses vary nontrivially as a function of correlation length, though they only study the W1 design and use only two correlation lengths (approximately 5 nm and 53 nm). They notice an increase in the loss rates for *all* frequencies as the correlation length is increased. Lastly, Minkov and Savona discuss another disorder model based on hole area fluctuations and show that the loss rates are largely unaffected by changing l_c, suggesting it to be a better model than the previous one. While we have not tested this model, it looks promising as an alternative model, yet it remains to be seen whether their conclusions also hold for DE PCWs.

VI. CONCLUSION

We have studied the behavior of disorder-induced losses as a function of correlation length using a quickly varying disorder model for three PCW designs. We found that the loss dependence on correlation length is dependent on both the phase and amplitude of the Bloch modes, which are highly dependent on the design and frequency of the bound propagation modes. In contrast to recent work [31], we find no significant changes in the loss spectrum as the correlation length is varied. Our studies also show the existence of a maximum loss given a finite correlation length for some frequencies and designs. Furthermore, using experimentally extracted values for surface roughness and correlation length, our calculations are in good agreement with experiments done on DE PCWs, as shown in Ref. [30]. However, there is always room for improvement in the models, and one effect that is potentially important is to account for is the disorder-induced changes in the band structure [39].

ACKNOWLEDGMENT

This work was supported by the Natural Sciences and Engineering Research Council of Canada.

[1] T. Baba, Nat. Photon. **2**, 465 (2008).
[2] T. F. Krauss, Nat. Photon. **2**, 448 (2008).
[3] J. Sancho, J. Bourderionnet, J. Lloret, S. Combrié, I. Gasulla, S. Xavier, S. Sales, P. Colman, G. Lehoucq, D. Dolfi, J. Capmany, and A. De Rossi, Nat. Commun. **3**, 1075 (2012).
[4] P. Colman, C. Husko, S. Combrié, I. Sagnes, C. W. Wong, and A. De Rossi, Nat. Photon. **4**, 862 (2010).
[5] C. Monat, M. Spurny, C. Grillet, L. O'Faolain, T. F. Krauss, B. J. Eggleton, D. Bulla, S. Madden, and B. Luther-Davies, Opt. Lett. **36**, 2818 (2011).
[6] J. Li, L. O'Faolain, and T. F. Krauss, Opt. Express **20**, 17474 (2012).
[7] P. Yao, V. S. C. Manga Rao, and S. Hughes, Laser Photon. Rev. **4**, 499 (2009).
[8] V. S. C. Manga Rao and S. Hughes, Phys. Rev. B **75**, 205437 (2007).
[9] A. Laucht, S. Pütz, T. Günthner, N. Hauke, R. Saive, S. Frédérick, M. Bichler, M.-C. Amann, A. W. Holleitner, M. Kaniber, and J. J. Finley, Phys. Rev. X **2**, 011014 (2012).
[10] T. Lund-Hansen, S. Stobbe, B. Julsgaard, H. Thyrrestrup, T. Sünner, M. Kamp, A. Forchel, and P. Lodahl, Phys. Rev. Lett. **101**, 113903 (2008).
[11] S. John, Phys. Rev. Lett. **58**, 2486 (1987).
[12] E. Yablonovitch, Phys. Rev. Lett. **58**, 2059 (1987).
[13] E. Kuramochi, M. Notomi, S. Hughes, A. Shinya, T. Watanabe, and L. Ramunno, Phys. Rev. B **72**, 161318 (2005).
[14] L. O'Faolain, T. P. White, D. O'Brien, X. Yuan, M. D. Settle, and T. F. Krauss, Opt. Express **15**, 13129 (2007).
[15] A. Parini, P. Hamel, A. De Rossi, S. Combrie, N.-V.-Q. Tran, Y. Gottesman, R. Gabet, A. Talneau, Y. Jaouen, and G. Vadala, J. Light. Technol. **26**, 3794 (2008).
[16] S. Hughes, L. Ramunno, J. F. Young, and J. E. Sipe, Phys. Rev. Lett. **94**, 033903 (2005).
[17] D. Gerace and L. C. Andreani, Opt. Lett. **29**, 1897 (2004).
[18] S. Johnson, M. L. Povinelli, M. Soljačić, A. Karalis, S. Jacobs, and J. D. Joannopoulos, Appl. Phys. B **81**, 283 (2005).
[19] B. Wang, S. Mazoyer, J. P. Hugonin, and P. Lalanne, Phys. Rev. B **78**, 245108 (2008).
[20] W. Song, R. A. Integlia, and W. Jiang, Phys. Rev. B **82**, 235306 (2010).
[21] K. K. Lee, D. R. Lim, H.-C. Luan, A. Agarwal, J. Foresi, and L. C. Kimerling, Appl. Phys. Lett. **77**, 1617 (2000).
[22] M. Patterson and S. Hughes, J. Opt. **12**, 104013 (2010).
[23] M. Patterson, S. Hughes, S. Schulz, D. M. Beggs, T. P. White, L. O'Faolain, and T. F. Krauss, Phys. Rev. B **80**, 195305 (2009).
[24] M. Patterson, S. Hughes, S. Combrié, N.-V.-Quynh Tran, A. De Rossi, R. Gabet, and Y. Jaouën, Phys. Rev. Lett. **102**, 253903 (2009).
[25] S. Mazoyer, J. P. Hugonin, and P. Lalanne, Phys. Rev. Lett. **103**, 063903 (2009).
[26] D. Marcuse, Bell Syst. Tech. J. **48**, 3187 (1969).
[27] F. P. Payne and J. P. R. Lacey, Opt. Quantum Electron. **26**, 977 (1994).
[28] L. Sapienza, H. Thyrrestrup, S. Stobbe, P. D. Garcia, S. Smolka, and P. Lodahl, Science **327**, 1352 (2010).

[29] M. Skorobogatiy, G. Bégin, and A. Talneau, Opt. Express **13**, 2487 (2005).
[30] N. Mann, S. Combrié, P. Colman, M. Patterson, A. De Rossi, and S. Hughes, Opt. Lett. **38**, 4244 (2013).
[31] L. O'Faolain, S. Schulz, D. M. Beggs, T. P. White, M. Spasenović, L. Kuipers, F. Morichetti, A. Melloni, S. Mazoyer, J. P. Hugonin, P. Lalanne, and T. F. Krauss, Opt. Express **18**, 27627 (2010).
[32] M. Minkov and V. Savona, Opt. Lett. **37**, 3108 (2012).
[33] N. Le Thomas, Z. Diao, H. Zhang, and R. Houdré, J. Vac. Sci. Technol. B Microelectron. Nanom. Struct. **29**, 051601 (2011).
[34] M. Patterson and S. Hughes, Phys. Rev. B **81**, 245321 (2010).
[35] M. Patterson, Master's thesis, Queen's University, Canada, 2009.
[36] S. Johnson and J. Joannopoulos, Opt. Express **8**, 173 (2001).
[37] S. G. Johnson, M. Ibanescu, M. A. Skorobogatiy, O. Weisberg, J. D. Joannopoulos, and Y. Fink, Phys. Rev. E **65**, 066611 (2002).
[38] A. Javadi, S. Maibom, L. Sapienza, H. Thyrrestrup, P. D. García, and P. Lodahl, Opt. Express **22**, 30992 (2014).
[39] N. Mann, A. Javadi, P. D. García, P. Lodahl, and S. Hughes, Theory and experiments of disorder-induced resonance shifts and mode edge broadening in deliberately disordered photonic crystal waveguides, arXiv:1505.02836.
[40] M. Born and E. Wolf, *Principles of Optics: Electromagnetic Theory of Propagation, Interference and Diffraction of Light*, 7th ed. (Cambridge University Press, Cambridge, 1999), p. 34.
[41] J. Li, T. P. White, L. O'Faolain, A. Gomez-Iglesias, and T. F. Krauss, Opt. Express **16**, 6227 (2008).
[42] P. Colman, S. Combrié, G. Lehoucq, and A. De Rossi, Opt. Express **20**, 13108 (2012).